Int J Clin Exp Pathol 2019;12(7):2405-2424
www.ijcep.com /ISSN:1936-2625/IJCEP0092441

Original Article

Amniotic epithelial cells reverse abnormal vascular structure and function in endometrial carcinoma

Liming Guan[1], Ai Zhang[2]

[1]*Department of Obstetrics and Gynaecology, Zhabei Central Hospital, No. 619, Zhonghuaxin Road, Jing'an District, Shanghai 200000, China;* [2]*Department of Obstetrics and Gynaecology, Shanghai Pudong New District People's Hospital, An Affiliate of Shanghai University of Medicine & Health Sciences, Shanghai 200000, China*

Received February 12, 2019; Accepted May 22, 2019; Epub July 1, 2019; Published July 15, 2019

Abstract: Background: The methods used to rebuild tumour vascular structure and function are called vascular normalization. Vascular normalization methods often block a single angiogenic molecular pathway, but tumor molecular pathways are interconnected and unstable. Since the vascular structure is not repaired, vascularity can be normalized only within a limited time. Amniotic epithelial cells (AECs) are used in tissue engineering to increase blood perfusion and promote wound healing. There have been no reports on the use of AECs in treatment to promote tumor vascular restoration. Methods: The multipotential stem cell features of AECs were detected by immunofluorescence (IF), RT-PCR, and western blot. A nude rat in situ endometrial carcinoma model was developed. AECs were transfected with lentivirus-green fluorescent protein (GFP)-luciferase (Luc). The vascular formation abilities of AECs were monitored in vitro and in vivo under different conditions. AECs were injected by the rat tail vein, tumour vascular structural and perfusion changes were monitored, and the synergistic effects of AECs with cisplatin (DDP) chemotherapy were evaluated. Results: AECs expressed the stem cell markers OCT4, Nanog, and CK19 at high levels. AECs could differentiate into adipocytes, chondrocytes, and osteocytes. Lentiviral GFP-Luc was successfully transfected into AECs, and GFP-labelled AECs formed vascular tube-like structures and invaded tumor tissue to form vascular structures in vitro. Kinetic luciferase imaging confirmed that AECs homed to rat uterine tumor tissues after injection by the tail vein. After AEC injection, tumour vascular α-SMA/CD31 labelling increased in vascular pericytes, while detection of VEGF-A expression by ELISA decreased. Cadherin labelling showed that basement membrane integrity improved distinctly in the AEC group compared with that in the corresponding control group. Hoechst 33342 and ultrasound Doppler detection showed that tumor vascular perfusion was ameliorated; pimonidazole perfusion showed reduced tumour tissue anoxia, and FITC-dextran perfusion confirmed that vascular leakage was obviously reduced in the AEC group compared with that in the control group. Tumor apoptosis and the rat survival rate in the AEC + DDP group were further enhanced, as demonstrated by CD31 (or α-SMA) IF and GFP colocalization, as well as GFP western blot. AECs differentiated into tumor vascular endotheliocytes or pericytes and enhanced tumor vascular integrity. Conclusion: AECs had the characteristics of pluripotent stem cells, and they could vascularize tissues under different conditions. AECs integrated into endometrial cancer vascular structures in nude rats, reduced dysregulated tumour angiogenesis, improved the efficiency of tumour vascular perfusion, and enhanced the cytotoxic effects of DDP. These findings provide a new method for the reconstruction of tumor vessels.

Keywords: Amniotic epithelial cells, tumour vascular restoration, vascular engineering

Introduction

Anti-vascular therapy is regarded as an important tumor treatment method, along with surgical excision and chemotherapy, but tumor starvation via anti-vascular therapy has proven unsatisfactory [1]. Clinical trials have found that chemotherapy following anti-vascular treatment can help patients with cancer survival longer. The explanation for this phenomenon is that anti-vascular agents improve the tumor vascular structure and perfusion function, allowing antitumor agents to more efficiently kill the tumor during treatment. Experimental results indicate that tumors have an abnormal vascular structure that easily leaks and has low perfusion. A major change in antitumor vascular strategy has occurred in recent years,

with a transition from blocking tumour vascular perfusion to restoring tumor vascularity and improving the tumour environment [2].

The methods of restoring tumor vascular structure and function often block a single angiogenic molecular pathway and ignore the fact that tumour molecular pathways are interconnected and unstable. Since the vascular structure is not repaired, the treatment effects are limited [2-4]. Amniotic epithelial cells (AECs) are used in tissue engineering to increase blood perfusion and promote wound healing [5]. There are no reports on the use of amniotic epithelial stem cells in "tumor vascular restoration".

AECs are derived from the placenta, and their telomerase activity is lost; thus, AECs have no risk of immunogenicity or tumorigenicity. AECs can be obtained following delivery of a baby, with no ethical challenges. Studies have shown that AECs possess stem cell features and can grow into 3 embryonic germ layers [5]. As a new source of multipotential stem cells, AECs can be used in the treatment of foetal pulmonary hypoplasia, tumour failure and insufficiency, and AECs from full-term pregnant placentas produce better effects [5]. AECs can implant into impaired tumour tissue, grow into granulosa cells, and repair tumor function. AECs can be also tracked by green fluorescent protein (GFP) and detected by markers, such as human nuclear antigens [6].

The first aim of this study was to evaluate the multipotential stem cell features of AECs to monitor the vascular formation abilities of AECs in vitro and in vivo under different conditions. The second aim of this study was to detect vascular morphologic and perfusion changes induced by AECs in rat endometrial cancer to determine whether vascular changes induced by AECs could enhance tumor DDP delivery and play a role in synergistic treatment effects.

Materials and methods

Placenta preparation and cell culture

Placentas were acquired from full-term pregnant women who required caesarean section, and patients who had syphilis or were HIV-I(+) were excluded. The study was approved by the ethics committee of Zhabei Central Hospital (No. 2017-98). All donors of placentas gave written consent to participate in the study. There were no conflicts of interest.

The detailed protocol for amniotic tissue isolation and AEC collection is shown in reference [6]. Briefly, amniotic membranes from the placentas were divided into fragments with diameters of 0.5 cm. The membrane fragments were separated by 0.20% trypsin at 37.2°C for 30 min. The separated cells were grown in DMEM supplemented with 15% foetal bovine serum, 100 U/mL streptomycin and 100 U/mL penicillin. The cell density was 4×10^6/dish (dish diameter 100 mm) in a humidified incubator with 5% CO_2 at 37.2°C. When the cells reached 80% confluence, they were used for subsequent experiments.

Lentivirus transfection and implantation of AECs

Lentivirus expressing both the GFP and luciferase genes was produced by 293T cells. The 293T cells were transfected with both the PLV-Firefly luciferase-GFP-Puro vector (Snapgene) and packaging vectors from the Lentieasy packaging mix (Genechem) for 24 h. Transfection was achieved with Lipofectamine 2000 (16 μg/100 mm dish). AECs (P3) were transfected with lentivirus from 293T cell supernatants collected for 3 days, and the process was enhanced by 5 μg/ml polybrene. Puromycin medium (6 μg/ml, optimal concentration) was used to select puromycin-resistant AEC clones, and the cells were cultured for 24 h. Infection efficiency was determined by the fluorescence intensity of GFP under a microscope and flow cytometric analysis for the expression level of GFP. When the ratio of infected cells was over 80%, the transfection process was terminated by 0.20% trypsin and 10% phosphate-buffered saline (PBS). The AECs were placed in culture medium again.

To embed AECs in nude rat tumor tissues, approximately 2.0×10^5 lentivirus-luciferase (Luc)-GFP-labelled AECs (1 ml) were injected by the rat tail vein on days one and four. In the control group, 1 ml of culture solution without AECs was administered by the tail vein at the same time.

Detection of differentiation

Differentiation of cultivated AECs into adipocytes, chondrocytes, and osteocytes was per-

formed in differentiation medium purchased from Shanghai Ziqi Biotechnology Co. Ltd. according to the manufacturer's instructions. Adipocyte differentiation was detected by oil red staining. Osteogenic differentiation was detected by alizarin red staining. Chondrocyte differentiation was detected by toluidine blue staining.

Detection of the formation of vascular tube-like structures in vitro

Matrigel was diluted 1:1 in serum-free medium, and 96-well plates were covered with 50 μL of Matrigel 356234. Matrigel was polymerized in an incubator at 37.0°C for 30 min. An AEC suspension 50 μl (10^4/well) was seeded into the plates and incubated in the incubator for 12 h; AECs were also cultured in combination with endometrial cancer cells. The growth of AEC vascular tube-like structures was observed and photographed under video and fluorescence microscopy every 30 min for 12 h.

Tumor model and treatment regimen

Healthy female rnu/+ nude rats (n = 120), 4-6 weeks old, 55-70 g, were used. All animal procedures were approved by the Institutional Animal Care and Use Committee of Shanghai and were performed in accordance with the National Research Council Guide for the Care and Use of Laboratory Animals. Efforts were made to minimize animal suffering and limit the number of animals used in the study.

Endometrial cancer cell line development and propagation

Development and propagation of the HEC-1b cell line was performed by general cell culture technology. The flash-frozen HEC-1b tumour line was thawed, and the cell suspension was stained with trypan blue to determine viability. The viability of the cells was greater than 95%. A suspension of 10^6 live cells/ml was mixed with normal saline at a 1:1 ratio, and 0.5 ml of the tumor suspension (concentration 3×10^7/ml) was injected into the lateral subcutaneous tissue of donor nude rats. Two to 3 weeks after implantation, the donor rats were sacrificed, and the subcutaneous abdominal tumors were excised and transected. Two 1- to 3-mm harvested tumor fragments were preserved for endometrial implantation. The remaining viable tumor was used to generate a cell suspension and injected into the subcutaneous abdominal tissue of another nude rat for propagation.

The endometrial cancer building process was performed as described in reference [7]: All surgical implantations were performed under aseptic conditions. The rats were anaesthetized with 3% pentobarbital sodium by a 30 mg/kg intraperitoneal injection. A laparotomy of 2 cm was created in the lower abdomen, exposing the bilateral uterus. One small stab incision was made by ophthalmic scissors approximately 0.5 cm deep in the anterior wall of the left midsection of the uterus, and the tumor pieces were placed into the endometrium with micro-forceps. The incision was sutured with 2-0 absorbable sutures in one layer. The abdomen was closed in one layer by 1-0 absorbable sutures. Then, the rats were aroused and returned to their cages. The rats were fed according to specific pathogen-free (SPF) animal requirements.

Tracking of luciferase-labelled AECs via an in vivo imaging system (IVIS)

The kinetic distribution of GFP-luc-AECs in rats was continuously monitored by IVIS (Perkin-Elmer) at 2 h, 12 h, 1 day, 2 days, 3 days, 7 days, 14 days, 21 days and 28 days after cell injection. D-Luciferin was intraperitoneally injected into the peritoneum of experimental rats after anaesthetization with pentobarbital sodium (50 mg/kg). Ten minutes later, the experimental rats were placed on the platform of an in vivo imaging dark box for image detection. The bioluminescent region was selected, and the number of photons in the region was calculated for quantitative analysis.

Tumor pathologic detection

The experimental rats were randomly divided into 2 groups (n = 30).

AEC group: (n = 15): A 1 ml suspension of GFP-Luc-labelled AECs (2.5×10^5 cells) was injected via the rat tail vein on days one and four.

Control group: (n = 15): For the control group, 1 mL of culture medium was administered by the rat tail vein one week after tumor embedding. The experimental rats were followed up every three days until 30 days to evaluate treatment

effects. At every time point, 3 rats were sacrificed, and tumor tissues were harvested.

The tumor tissues were fixed in 10% formaldehyde, paraffin-embedded and continuously sectioned at a thickness of 5 μm. Haematoxylin and eosin (H&E) staining was performed to observe the tumor vascular structure under light microscopy.

Immunohistochemical detection

AECs were fixed with 10% formalin, permeabilized with 0.1% Triton X, and blocked with blocking buffer. Then, the AECs were incubated with primary antibodies (Abs) specific for OCT4, NANOG, VASA, DAZL, STELL, and CD117 for 2 h at approximately 15°C.

Rat endometrial cancer tissues from the AEC group and the control group were fixed in 10% formalin, embedded in paraffin, sectioned, and placed on slides. The slides were blocked with blocking buffer and detected by primary Abs specific for GFP, CD31, Ki67, and α-SMA following the manufacturer's instructions.

Then, cells or sections were detected by the following secondary Abs: FITC-labelled IgG or rhodamine-labelled IgG.

The following indices were quantified: microvessel density (MVD), tumor cell proliferation, endothelial cell coverage, and nuclear density. Microvessel density (MVD) was determined according to CD31 detection. The details are provided in reference [3].

The percentage of α-SMA-stained vasculature was determined according to the same methods.

The vessel maturation index (VMI) was defined as the ratio of α-SMA-stained vasculature to CD31-stained vasculature.

Tumor vascular leakage and perfusion

Capillary leakage was detected by administration of FITC-dextran (2 mg/rat) by the tail vein before the tumors were resected. The tissues were fixed with 10% formalin, and cryosections were made for fluorescence microscopy.

Vascular perfusion was evaluated by Hoechst 33342 dye (65 mg/kg) before tumor resection. Biotinylated lectin (0.12 mg/rat) was administered before the animals were sacrificed.

The vascular perfusion fraction was defined as the ratio of biotinylated lectin detected to CD31 labelling.

Imaging of each marker was performed by a fluorescence microscope. Each marker was quantified by Photoshop color gradation from 1 to 255 units. The positively labelled or double positively labelled imaging data were analysed by MATLAB with an internal piecewise algorithm.

Color doppler flow imaging (CDFI)

Nude rats (n = 30) were randomly divided into two groups: the AEC group and the control group. CDFI detection was performed every three days for 30 days to determine changes in tumor vascular perfusion.

VEGF-A enzyme-linked immunosorbent assay (ELISA) detection

Rats were randomly divided into AEC and control groups (n = 16 each group). After AECs were administered, the rats were sacrificed, and tumor tissues were harvested and fixed in liquid nitrogen every other day until nine days. Tumor tissues were dissociated by Tissue Lyser. VEGF ELISA was used to detect lysed protein levels according to the manufacturer's instructions.

Treatment with AECs and cisplatin

The synergistic effects of AEC and cisplatin (cis-dichlorodiammine platinum, DDP) were compared and monitored (n = 30 for each group). DDP was purchased from Shanghai First Biochemical Pharmaceutical Co. Ltd. The rats in the treated groups were subjected to AEC injection by the tail vein on days one and four, as described above, and/or DDP by abdominal administration (4.0 mg/kg diluted to 1 ml in saline), while the control group was treated with the same amount of saline (1 ml). Combination treatment groups were given DDP 2 days before AECs, AECs 2 days before DDP, or DDP simultaneously with four doses of AECs on day one and day four. The synergistic effects of AECs and DDP were evaluated by using different doses and different administration schedules for the two agents.

Table 1. Primer sequence for real-time PCR of AEC stem cell markers

Gene	Primer sequence 5'→3'		Amplicon size (bp)
Oct4	Forward	CGAGCAATTTGCCAAGCTCCTGAA	396
	Reverse	TTCGGGCACTGCAGGAACAAATTC	
Nanog	Forward	TTCCTTCCTCCATGGATCTG	213
	Reverse	TCTGCTGGAGGCTGAGGTAT	
SOX2	Forward	GCCGAGTGGAAACTTTTGTC	264
	Reverse	GTTCATGTGCGCGTAACTGT	
E-cadherin	Forward	TGAGCTTGCGGAAGTCAGTT	219
	Reverse	ACCGTGAACGTGTAGCTCT	
N-cadherin	Forward	CGCCATCCGCTCCACTT	227
	Reverse	GGACTCGCACCAGGAGTAAT	
Vimentin	Forward	CTCTGGCACGTCTTGACCTT	231
	Reverse	ACCATTCTTCTGCCTCCTGC	
CK19	Forward	AGGTGGATTCCGCTCCGGGC	461
	Reverse	ATCTTCCGTCCCTCGAGCA	
Snail	Forward	CTCGGACCTTCTCCCGAATG	223
	Reverse	TCATCAAAGTCCTGTGGGGC	
β-actin	Forward	TCGCCTTTGCCGATCC	202
	Reverse	GAATCCTTCTGACCCATGCC	

The ratio of cell proliferation was defined as the fraction of Ki67-positive nuclei divided by total nuclei within the tumor tissue region.

Tumor sizes were detected by Vernier callipers every three days. The tumor volume (V) was counted according to "$V = A \times B^2/2$" (A represents the maximum diameter, B represents the transverse diameter). When the tumor diameter was approximately 0.5 cm, the experimental rats received treatment. A comparison of the tumor volume was made between the start of treatment and the end of treatment.

Real-time RNA detection

Total RNAs were isolated from cultured cells by a total cellular RNA isolation kit (Beijing Solaibao Technology Co. Ltd.). Then, the RNAs from the samples were reverse transcribed using a Takara reverse transcription kit. Real-time quantitative PCR was performed by an R&D Biosystems real-time PCR instrument. The cDNA samples were labelled by SYBR Green. The markers included OCT4, NANOG, CD117, and 18S RNA. According to temperature differences, PCR detection mainly included three steps: degeneration, annealing, and extension. The primer sequences are listed in **Table 1**. The process was performed for 30 cycles according to the manufacturer's instructions. Gene expression levels were evaluated using the $2^{-\Delta\Delta Ct}$ method. β-actin was used as an internal reference.

TUNEL analysis

Cell death (apoptosis) in tumor tissue was detected with transferase-mediated deoxyuridine triphosphate-biotin nick end labelling (TUNEL) and 4,6-diamino-2-phenyl indole (DAPI) following the manufacturer's protocols. The tumor sections were observed under fluorescence microscopy.

Western blot analysis

AECs and tumor specimens were lysed in RIPA lysis buffer. The material formed by the lysis of cells was separated by centrifugation at 12,000 revolutions per minute. The supernatant was collected. Electrophoresis was performed on a sodium dodecyl sulfate polyacrylamide gel. The electrophoresed products were transferred to nitrocellulose membranes. The primary Abs used in this study included Nanog (rabbit anti-human 1:200, Abcam); Oct-4 (rabbit anti-human 1:200, Santa Cruz); CK19 (mouse anti-human 1:100, Invitrogen); Snail (goat anti-human antibody 1:250, Abcam); CD117 (mouse anti-human 1:100, Biolegend); Rex-1 (rabbit anti-human antibody 1:150, Abcam); and SSEA4 (mouse anti-human antibody 1:100, R&D Systems). The secondary Abs were conjugated to horseradish peroxidase, and protein production was detected by western blot detection reagents (Thermo Fisher Scientific). β-Actin was used as an internal reference.

Statistical analysis

The quantitative variables in this study were presented as the mean ± SD, and one-way analysis of variance (ANOVA) was used to analyse the differences between groups. Qualitative variables were represented as percentages (%), and the chi-square test was used to evaluate the effects of different groups. The data were analysed by GraphPad software 6.0.

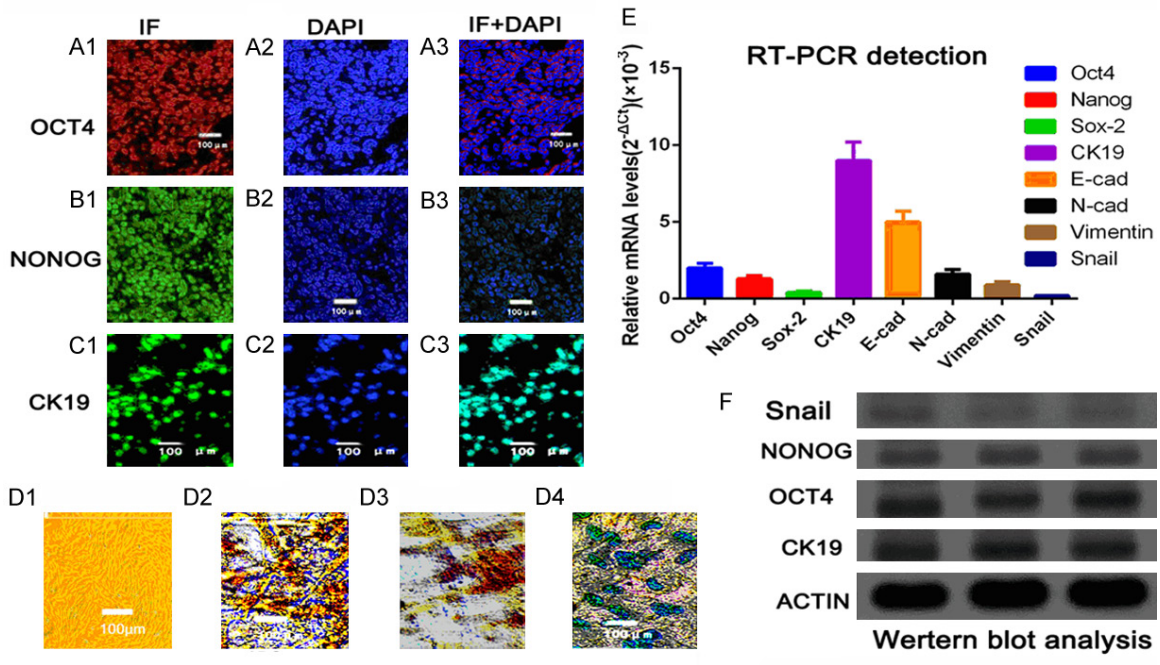

Figure 1. AEC stem cell feature evaluation. A1-C3. Immunofluorescence staining of AECs for the stem cell markers Oct4, Nanog and CK19 was positive. D1. The shape of AECs. D2. AEC adipocyte differentiation, oil red staining. D3. AEC osteogenic differentiation, alizarin red staining. D4. AEC chondrocyte differentiation, toluidine blue staining. E. RT-PCR detection. AECs expressed Oct-4, Nanog, CK19 and E-cadherin at high levels; N-cadherin, Vimentin and Snail were expressed at low levels. F. Western blot analysis. The Oct4, Nanog and CK19 proteins were expressed at high levels, and the Snail protein was expressed at very low levels.

Confidence intervals of 95% were considered statistically significant. The significance level was set at p less than 0.05.

Results

Evaluation of the multipotential stem cell features of AECs

The features of AECs were detected by real-time PCR, immunofluorescence staining and western blot. Immunofluorescence labelling showed that AECs were positive for the pluripotent stem cell markers Oct4 and Nanog. The cells were also positive for the epithelial marker cytokeratin (CK19) (**Figure 1A1-C3**). RT-PCR detection showed that AECs were positive for the stem cell markers Oct-4 and Nanog. The epithelial markers CK19 and E-cadherin were expressed at high levels.

AECs were induced to differentiate into adipocytes, chondrocytes, and osteocytes. Adipocyte differentiation was detected by oil red staining. Osteogenic differentiation was detected by alizarin red staining. Chondrocyte differentiation was detected by toluidine blue staining (**Figure 1D1-D4**).

The mesenchymal cell markers N-cadherin and vimentin were expressed at low levels according to RT-PCR analysis. Almost no positive expression was detected for the Snail gene (see **Figure 1E**). Protein expression was high for Oct4, Nanog and CK19, as indicated by Western blot analysis (**Figure 1F**). This result was consistent with the immunofluorescence staining results and the mRNA gene expression results obtained from RT-PCR analysis. All these data showed that AECs had stem cell characteristics.

GFP-Luc-AEC labelling and tracking

The structure of the PLV-Firefly luciferase-GFP-Puro vector is shown in **Figure 2A1**. The lentiviral AEC transfection efficiency was determined by GFP expression under a fluorescence microscope (see **Figure 2A2**). The percentage of GFP transfection was analysed by flow cytometry, and the GFP transfection rate was 4.4 ± 0.5% in the mock group (empty vector transfected) versus 95.6 ± 1.6% in the AEC group (see **Figure 2A3**). IVIS imaging showed luciferase expression in a culture plate covered by AECs (**Figure 2A4**, **2A5**). This finding demonstrated

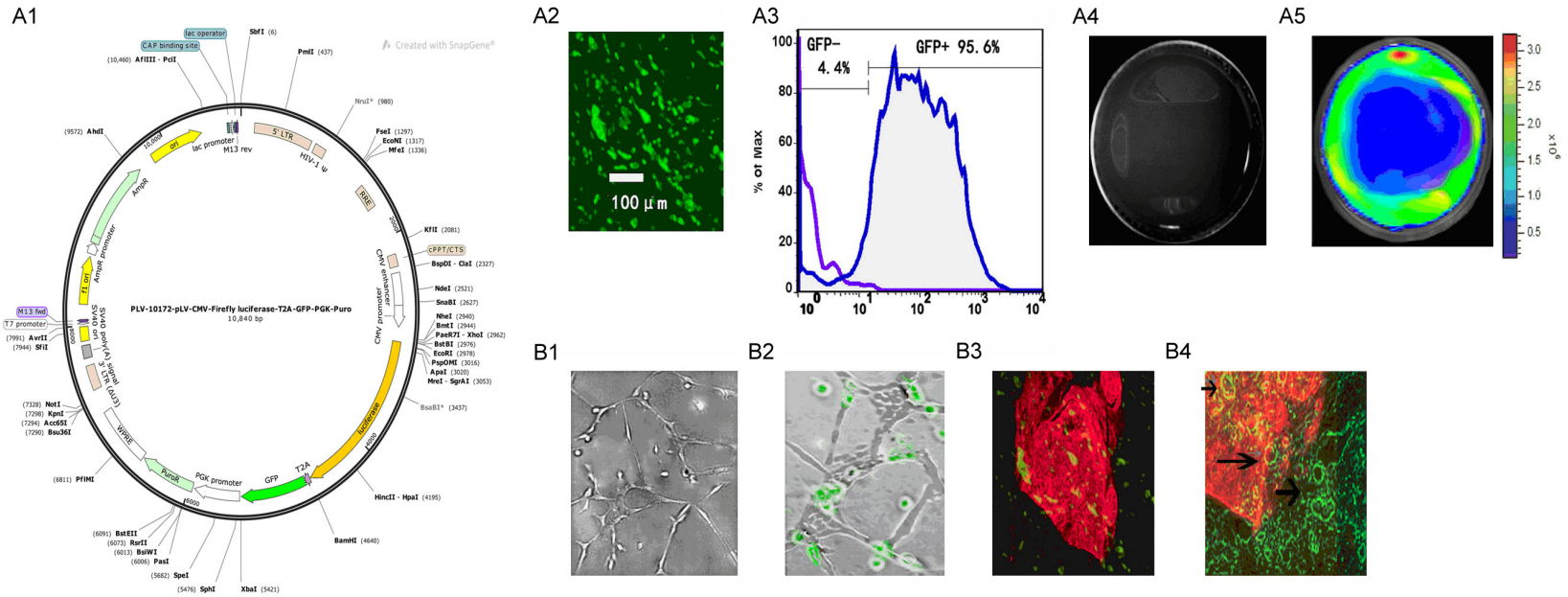

Figure 2. Lentiviral AECs were transfected and tracked in vitro. A1. The PLV-Firefly luciferase-GFP-Puro vector structure. A2. Lentiviral AEC transfection efficiency was determined by GFP fluorescence. A3. Lentiviral GFP transfection efficiency was analysed by flow cytometry. A4, A5. IVIS imaging of luciferase expression(+) in a plate covered by GFP-Luc-AECs. B1, B2. AECs formed vascular tube-like structures and were tracked by GFP in vitro. B3, B4. AECs invaded tumor spheroids to form vascular structures and were tracked by GFP (indicated by arrow) in vitro.

that lentiviral GFP-Luc was successfully transfected into AECs.

AEC vascular tube-like structure formation in vitro

AECs formed vascular tube-like structures and invaded tumor spheroids to form vascular structures in vivo (**Figure 2B1-B4**).

Tracking of luciferase (Luc)-labelled AECs by IVIS imaging

The rats were injected with 5×10^5 AECs (1 ml) by the tail vein, and 1 ml of saline was administered in the control group. Luciferin was injected into the peritoneum of experimental rats. Luciferase reporter gene expression in the rats was monitored via an IVIS. The dynamic distribution of AECs implanted in nude rats was tracked in both the supine and prone positions.

The luciferase signal intensities of all the rats in the experimental group were similar, and the overall signal intensity decreased with time. The luc signals were detected in the lungs of the rats 2 h after AEC injection, diffused along the ventral and dorsal sides within 2 to 14 days, and reached the lower abdomen and uterus. The chest signals became attenuated and were undetectable on the third day. Luciferase signals increased within 2 to 7 days and reached a peak on the 7th day, including the hypogastrium and uterus, but the peak level was significantly lower than the photon quantity in the lungs within the first 24 h. Biological signals in the whole body became blurry and disappeared 21 days later. The kinetic imaging changes after AEC injection are shown in **Figure 3A1-A10**. No bioluminescent signals appeared on IVIS in the control group during the entire experimental process (see **Figure 3A11**).

Dynamic changes in luciferase luminescence intensity are shown in **Figure 3B**.

The experimental animals were euthanized, and uterine tumor samples were collected on the 15th day. IVIS images showed positive luciferase expression in uterine tumor samples (see **Figure 3C1**, **3C2**).

This finding proved that AECs may home to rat uterine tumor tissues after injection by the tail vein. Next, we explored whether AECs could affect uterine tumor vascular structure and perfusion function.

AECs restored the tumor vasculature

Morphologic changes of the tumor vasculature: We evaluated the effect of AECs on vascular structure in an implanted endometrial cancer nude rat model. The rats were injected with 5×10^5 AECs (1 ml) by the tail vein, and 1 ml of saline was administered in the control group.

Tumor microvessel density and pericyte coverage: One week after AEC injection, the tumor vessel density detected by CD31 was evaluated. The average CD31 expression was 6.3 ± 1.3 in the AEC group versus 15.4 ± 2.4 in the control group (**Figure 4A**, **4B**). Pericyte coverage was detected by α-SMA staining. The average α-SMA labelling was 27.5 ± 1.3 in the AEC group versus 6.3 ± 1.4 in the control group (see **Figure 4C**, **4D**). The α-SMA/CD31 labelling (VMI) was 0.48 ± 0.2 in the AEC group versus 4.58 ± 0.3 in the control group.

CD31 expression was significantly reduced in the AEC group compared with that in the control group. α-SMA labelling increased significantly in the AEC group compared with that in the control group. Therefore, the ratio of α-SMA/CD31 (VMI) increased significantly in the AEC group compared with that in the control group (two-way ANOVA, $F(2,84) = 950.2$, $P<0.0001$, $n = 16$ each group) (see **Figure 4E**). This finding proved that the vascular structural integrity was increased. The number of mature vessels increased, and the number of immature vessels decreased.

VEGF-A detection: Four days after AEC injection, tumor VEGF-A expression, as detected by ELISA labelling, decreased distinctly in the AEC group over compared with that in the control group (two-way ANOVA, $F(5,168) = 3.478$, $P = 0.0051$, $n = 16$ each group) (**Figure 4F**). This finding indicated that AECs reduced abnormal hyperplasia of tumor vessels.

Western blot analysis of cadherin expression: Cadherin expression was detected by western blot, and the content of cadherin increased significantly in the AEC group compared with that in the control group (paired t test, $P = 0.0071$, $t = 11.77$, $n = 16$ each group) (**Figure 4G**, **4H**).

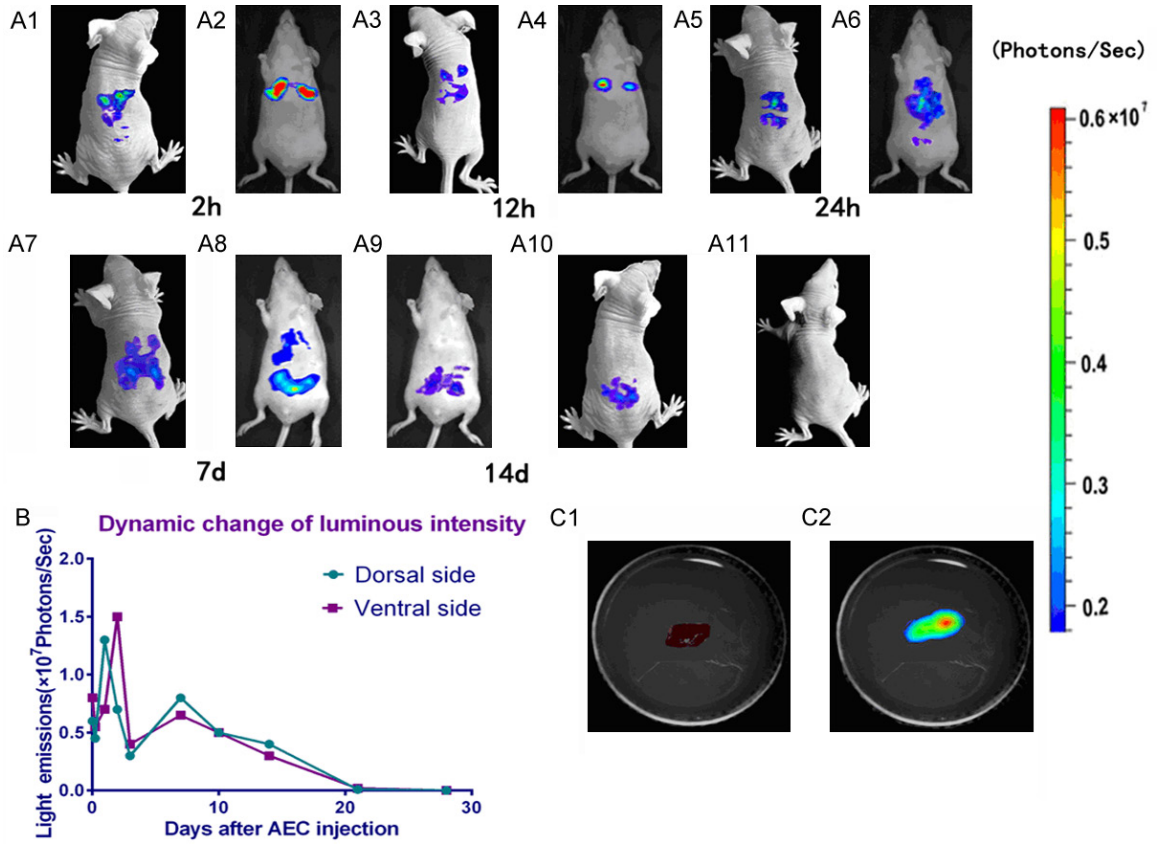

Figure 3. Tracking of luciferase (Luc)-labelled AECs by IVIS imaging. A1-A10. The kinetics of bioluminescent signal changes after AEC injection were tracked by IVIS. The luc signals were detected in the lungs of rats after AEC injection for 2 h, diffused along the ventral and dorsal sides within 2 to 14 days, and reached the lower abdomen and uterus. The whole body signals disappeared 21 days later. A11. No bioluminescence signals appeared on IVIS in the control group during the entire experimental process. B. Dynamic changes in luciferase luminescence intensity. C1. A rat uterine tumor sample collected on the 15th day after AEC injection. C2. IVIS imaging showed luciferase expression(+) in the above uterine tumor sample.

This finding indicated an increase in tumor vascular integrity.

Vascular perfusion changes caused by AECs

Vascular perfusion improvement and hypoxia reduction: To evaluate the vascular restorative effects of AECs, tumor vascular perfusion improvements and tumor hypoxia reduction were monitored. The relative levels of lectin, CD31 and lectin/CD31 were 6.0 ± 0.5 versus 13.0 ± 1.40, 12 ± 0.7 versus 11.0 ± 1.3, and 0.42 ± 0.1 versus 1.10 ± 0.11 in the control group and AEC group, respectively. The relative levels of lectin and lectin/CD31 in the AEC group increased obviously compared with those in the control group (two-way ANOVA, $F(2,42) = 133.3$, $P<0.0001$, $n = 15$ for each group) (see **Figure 5A1**, **5A2**).

The lectin/CD31 ratio increased via MATLAB analysis, as shown in the schematic diagram (see **Figure 5D**). There was a significant difference between the control and AEC groups.

Hoechst 33342 injection for vascular perfusion was performed in the peritumor and intratumor regions. The average Hoechst 33342 perfusion fraction was 68 ± 5.5 versus 93.5 ± 6.7 in the control group and the AEC group, respectively. The vascular perfusion fraction was significantly increased in the AEC group compared with that in the control group (two-way ANOVA, $F(1,28) = 21.32$, $P<0.0001$, $n = 15$ each group) (**Figure 5B1-B4**).

The vascular perfusion fraction was analysed by MATLAB as shown in the schematic diagram (see **Figure 5E**). There was a substantial difference between the control and AEC groups.

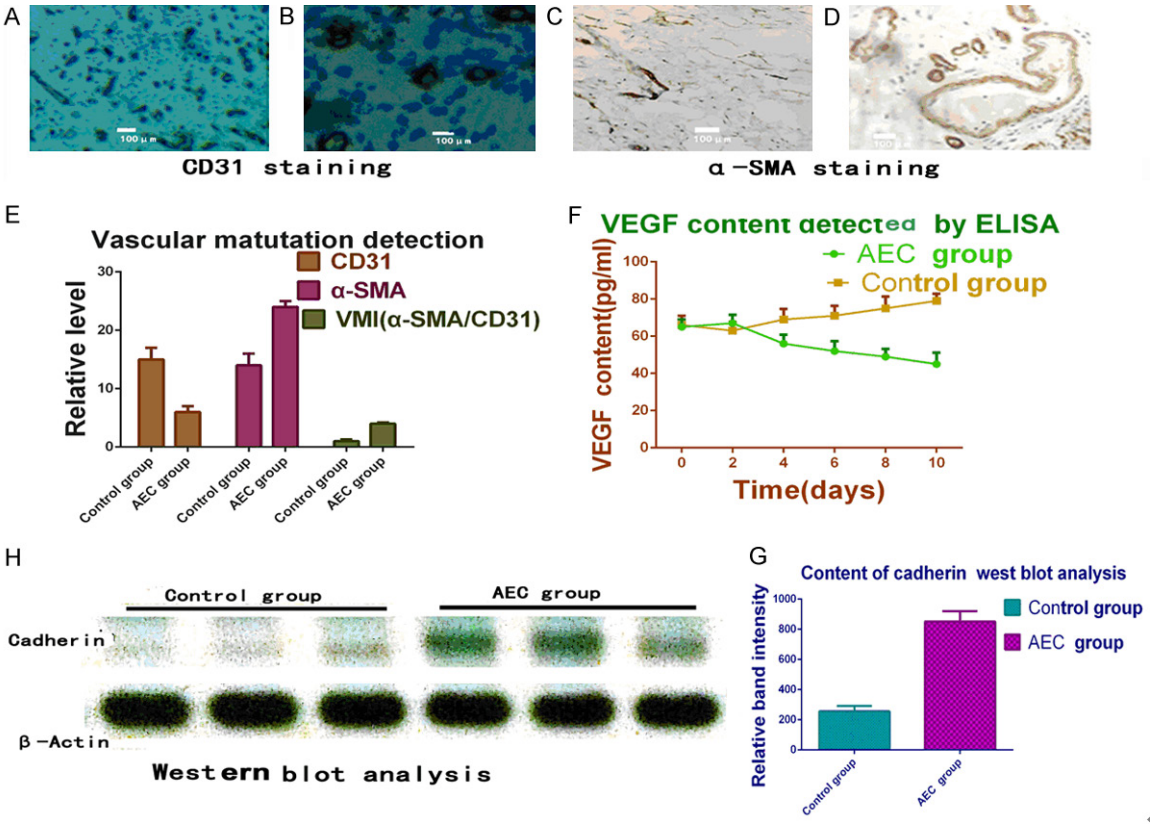

Figure 4. AECs improved tumor vascular integrity. A. Tumor vessel density labelled by CD31 in the control group. B. CD31 expression was reduced in the AEC group, and vascular endothelial integrity was enhanced. C. Pericyte coverage was labelled by α-SMA staining in the control group. D. α-SMA expression and pericyte coverage increased. E. Expression level of CD31, α-SMA and the α-SMA/CD31 ratio are presented as a schematic diagram. F. VEGF-A expression detected by ELISA decreased in the AEC group compared with the control group. G, H. Western blot analysis of cadherin expression was significantly enhanced in the AEC group compared with the control group, indicating an increase in tumor vascular integrity.

These results demonstrate that AECs improve tumor vascular perfusion function.

Pimonidazole perfusion for hypoxia detection was performed outside and inside the tumor. The average hypoxic region was 8.4 ± 2.7% and 23.5 ± 4% in the AEC and control groups, respectively. The hypoxic region decreased distinctly in the AEC group compared with that in the control group (two-way ANOVA, $F(1,28) = 560.8$, $P<0.0001$) (**Figure 5B1-B4**, **5F**). There was a significant difference between the control and AEC groups. This finding confirmed that AECs reduced hypoxia in rat uterine tumors.

FITC-dextran perfusion detected tumor vascular leakage in the control group and AEC group (**Figure 5C1**, **5C2**). The level of FITC-dextran labelling decreased in the AEC group compared with that in the control group, and the difference was significant (unpaired t test, $P<0.0001$, $t = 19.36$) (see **Figure 5G**).

Ultrasonic CDFI observation: Ultrasonic CDFI showed a few blood flow signals around and inside the tumor tissue in the control group (see **Figure 5H1**, **5H3**). One week after AEC injection, ultrasonic CDFI found more dotted, linear, or cyclic vascular blood flow signals peripheral to and within tumor nodules in the AEC group. This finding indicated that vascular perfusion increased significantly in the AEC group compared with that in the control group (**Figure 5H2**, **5H4**). Ultrasonic detection further confirmed that AECs could improve tumor vascular perfusion.

DDP inhibition of tumor growth

The rats were injected with 5×10^5 AECs by the tail vein and administered 4.0 mg/kg DDP via

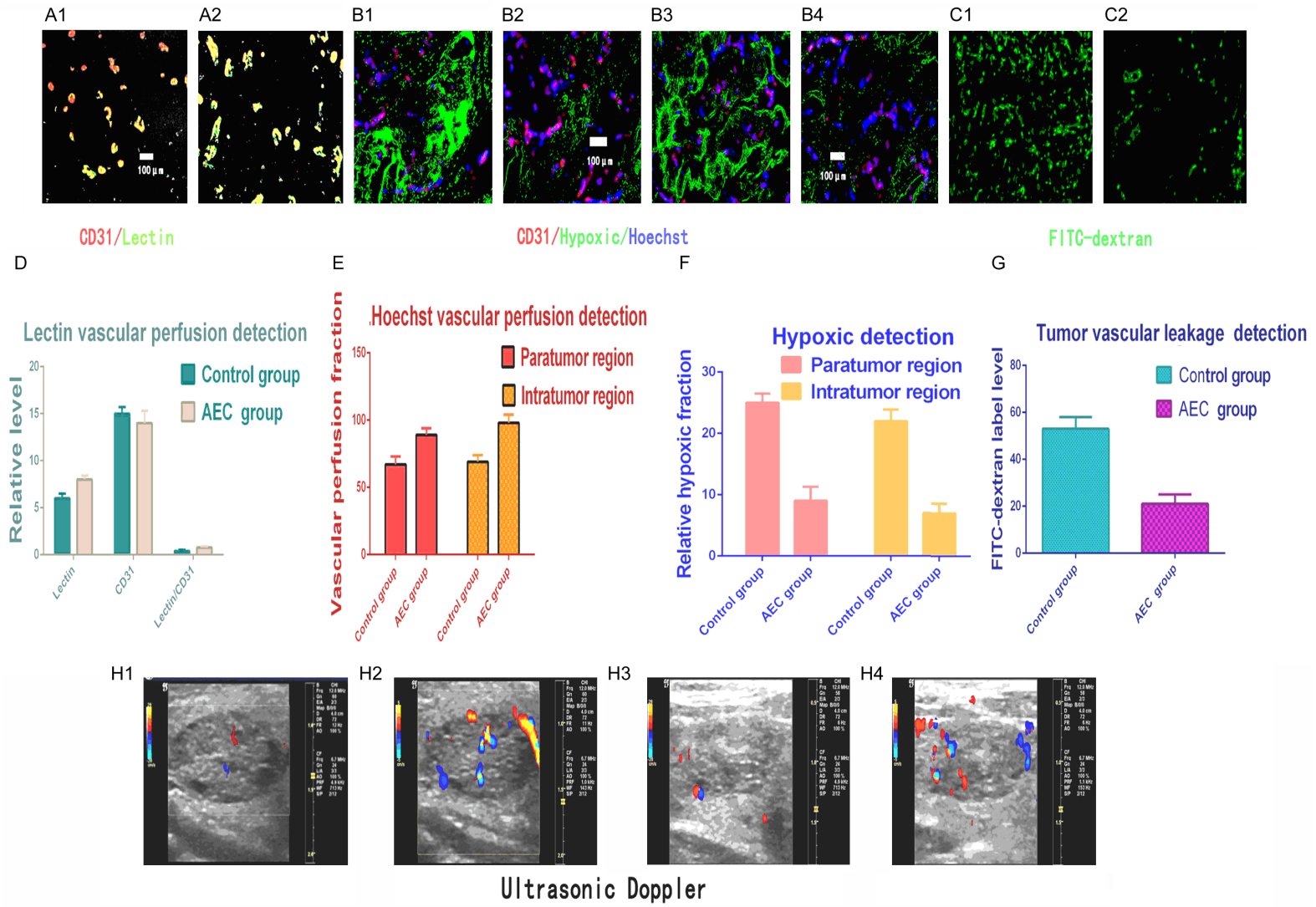

Figure 5. AECs increased tumor vascular perfusion and reduced hypoxia. A1, A2. Tumor lectin, CD31 immunofluorescence double staining, and lectin labelling intensity increased in the AEC group compared with the control group. D. Lectin/CD31 ratio after MATLAB analysis. B1-B4. Tumor perfusion was enhanced in the AEC group compared with the control group, while tumor hypoxia declined in the AEC group compared with the control group. E. Vascular perfusion fraction by MATLAB analysis. F. Tumor hypoxia by MATLAB analysis. C1. Tumor vascular leakage in the control group, with FITC-dextran perfusion detection. C2. Tumor vascular leakage was obviously reduced in the AEC group compared with the control group, with FITC-dextran perfusion detection. G. Tumor vascular leakage by MATLAB analysis. H1, H3. Ultrasonic CDFI showed a few blood flow signals peripheral to and inside the tumor tissue in the control group. H2, H4. Ultrasonic CDFI found more vascular blood flow signals around and inside tumor nodules in the AEC group.

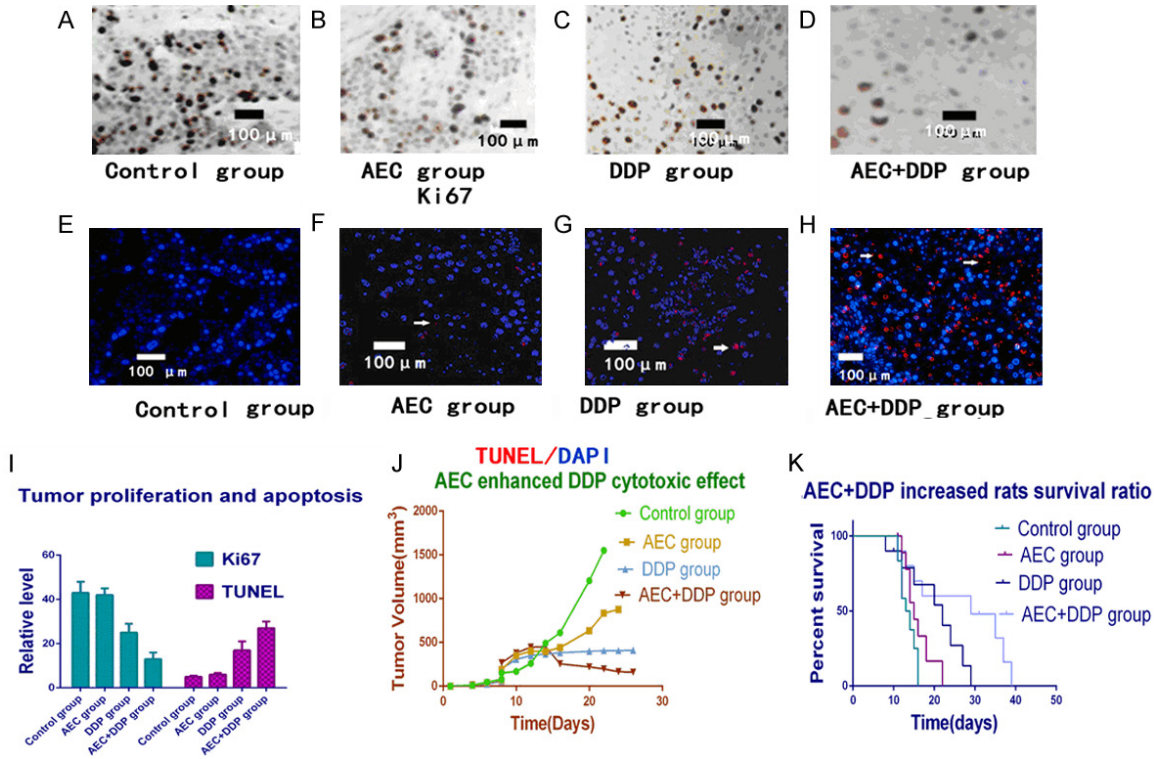

Figure 6. AECs enhanced the cytotoxic effects of DDP on tumor-bearing rats. (A-D) Tumor proliferative ratio detected by Ki67. The proliferative ratio was partially reduced in the AEC group (B) and the DDP group (C) compared with the control group. The proliferative ratio was significantly reduced in the AEC + DDP group (D). (E-H) Tumor apoptosis labelled by TUNEL. A few apoptotic bodies appeared within tumor cells after AEC injection (F). A number of apoptotic bodies appeared within tumor cells in the DDP group (G). The number of apoptotic bodies obviously increased in the AEC + DDP group (H). (I) The diagram shows tumor proliferation inhibition and apoptotic status. (J) The diagram showed that the tumor volume growth ratio was slightly reduced in the AEC group and the DDP group, and the tumor volume was distinctly reduced in the AEC + DDP group compared with the control group. (K) The diagram showed that the rat survival rate was slightly enhanced in the AEC group and the DDP group compared with the control group, and the survival rate was increased distinctly in the AEC + DDP group compared with the other three groups, which confirmed that AEC enhanced the cytotoxic effects of DDP.

abdominal administration or 1 ml saline injection in the control group for 4 weeks.

The tumor proliferation ratio detected by Ki67 was 43.46 ± 4.54% in the control group, 41.38 ± 2.52% in the AEC group, 24.56 ± 2.24% in the DDP group, and 16.35 ± 3.42% in the AEC + DDP group 9 days later. The proliferative percentage was slightly higher in the AEC group than in the control group, but there was no significant difference between the control and AEC groups. The proliferative ratio was significantly reduced in the DDP group compared with that in the control group (one-way ANOVA, n = 8 each group, $F(3,28) = 126.6$, $P<0.0001$) (see **Figure 6A-D**).

Tumor apoptosis labelling by TUNEL was 5.37 ± 0.5% in the control group, 6.26 ± 0.47% in the AEC group, 17.49 ± 3.54% in the DDP group, and 24.57 ± 5.48% in the AEC + DDP group 9 days later. Tumor apoptosis increased in the DDP group ((one-way ANOVA, n = 8 each group, $F(3,28) = 63.69$, $P<0.0001$) (see **Figure 6E-H**).

Tumor proliferation inhibition and apoptotic status are presented in the schematic diagram in **Figure 6I**.

Tumor volume growth was monitored by ultrasonic examination and rat autopsy every three days. Tumor volume changes are presented in the schematic diagram. Curves of tumor volume growth are shown in **Figure 6J**. The tumor volume growth ratio was slightly reduced in the AEC group and the DDP group, and the tumor volume was distinctly reduced in the AEC + DDP group compared with that in the control group.

The survival rate of the experimental rats is shown in a schematic diagram. The curves of the rat survival rate are shown in **Figure 6K**. The rat survival rate was slightly enhanced in the AEC group and DDP group compared with that in the control group, indicating that the rat survival rate in the DDP group increased distinctly compared with that in the control group (log rank test, $\chi^2 = 14.68$, $P = 0.0001$, $n = 8$ each group). This finding confirmed that DDP administration significantly inhibited tumor growth.

Synergistic treatment effect of AEC + DDP

As mentioned above, the effects of AEC and DDP were monitored, and the tumor proliferation rate detected by Ki67 labelling in the AEC + DDP group decreased significantly compared with DDP alone at a dose of 4.0 mg/kg. Therefore, AECs at a dose of 5×10^5 cells injected before DDP application promoted a cytotoxic effect compared with simple DDP injection. DDP at a dose of 4.0 mg/kg inhibited tumor growth significantly less than the AEC + DDP. The same dose of DDP appeared to have a weaker treatment effect without previous AEC injection, as shown in **Figure 6E-H**.

When detecting tumor volume every three days, the volume of AEC + DDP-treated tumors was distinctly reduced compared to that of the control group 9 days after the beginning of treatment (see **Figure 6I**). In contrast, the surviving proportion of experimental animals in the AEC + DDP group increased distinctly compared with that of the other groups (see **Figure 6K**).

In summary, the tumor proliferation rate and tumor volume further declined in the AEC + DDP group. Tumor apoptosis and the rat survival rate in the AEC + DDP group were further enhanced. This finding proved that AECs enhanced the cytotoxic effect of DDP on endometrial carcinoma. This effect corresponded to the tumor vascular morphology and perfusion normalization induced by AECs.

AEC-GFP labelled cells implanted into rat tumor tissue

To verify whether GFP-labelled cells in recipient tumors were derived from injected AECs, the rats were sacrificed, and uterine tumor specimens were collected. Double immunofluorescence labelling with GFP and CD31 or GFP and SMA was performed to track the changes in AECs after injection from 5 to 30 days. After one week of AEC injection, the GFP(+) marker presented an uneven punctate distribution within tumor stromal tissues in the AEC group. After 2-3 weeks, GFP(+) cells appeared in the tumor tissue close to vessels. Finally, GFP(+) cells were detected around sites of tumor vascularity.

The tumor vascular network was twisted, and the vascular structure was incomplete in the control group. Only CD31 labelling was positive, and no GFP(+) cells were detected in the control group (see **Figure 7A1**).

In the AEC group, GFP(+) cells were mixed with haemocytes within the tumor microvascular cavity. GFP(+) cells were integrated with endotheliocytes in the tumor microvascular wall, and vascular structural integrity was enhanced. GFP and CD31(+) cells were colocalized with vascular network mural cells (see **Figure 7A2-A4**). The percentage of twisted vessels was 34 ± 5% versus 23 ± 1.4% in the control group and AEC group, respectively. There was a significant difference between the two groups (two-way ANOVA, $F(1,56) = 8.976$, $P = 0.0041$, $n = 15$ for each group) (see **Figure 7F**).

Tumor vessels sprouted to form new vessels, and endotheliocyte monolayers formed sites of vascularity. These vascular structures were incomplete in the control group. Only CD31 labelling was positive, and no GFP(+) cells were detected in the control group (see **Figure 7B1**).

In the AEC group, GFP(+) cells were integrated with tumors sprouting angiogenic vascularity and endotheliocyte monolayers forming vascularity. GFP and CD31 double staining was positive (see **Figure 7B2-B4**). The percentage of monolayer endotheliocytes forming intact vessels was 12 ± 2% versus 35 ± 4% in the control group and AEC group, respectively. There was a significant difference between the two groups (two-way ANOVA, $F(1,56) = 52.90$, $P<0.0001$, $n = 15$ for each group). There was an obvious difference between the two groups (see **Figure 7F**).

Only CD31(+) endotheliocyte monolayer vascularity was found in the control group. Arrows indicate vascular wall defects by CD31 staining (see **Figure 7C1**).

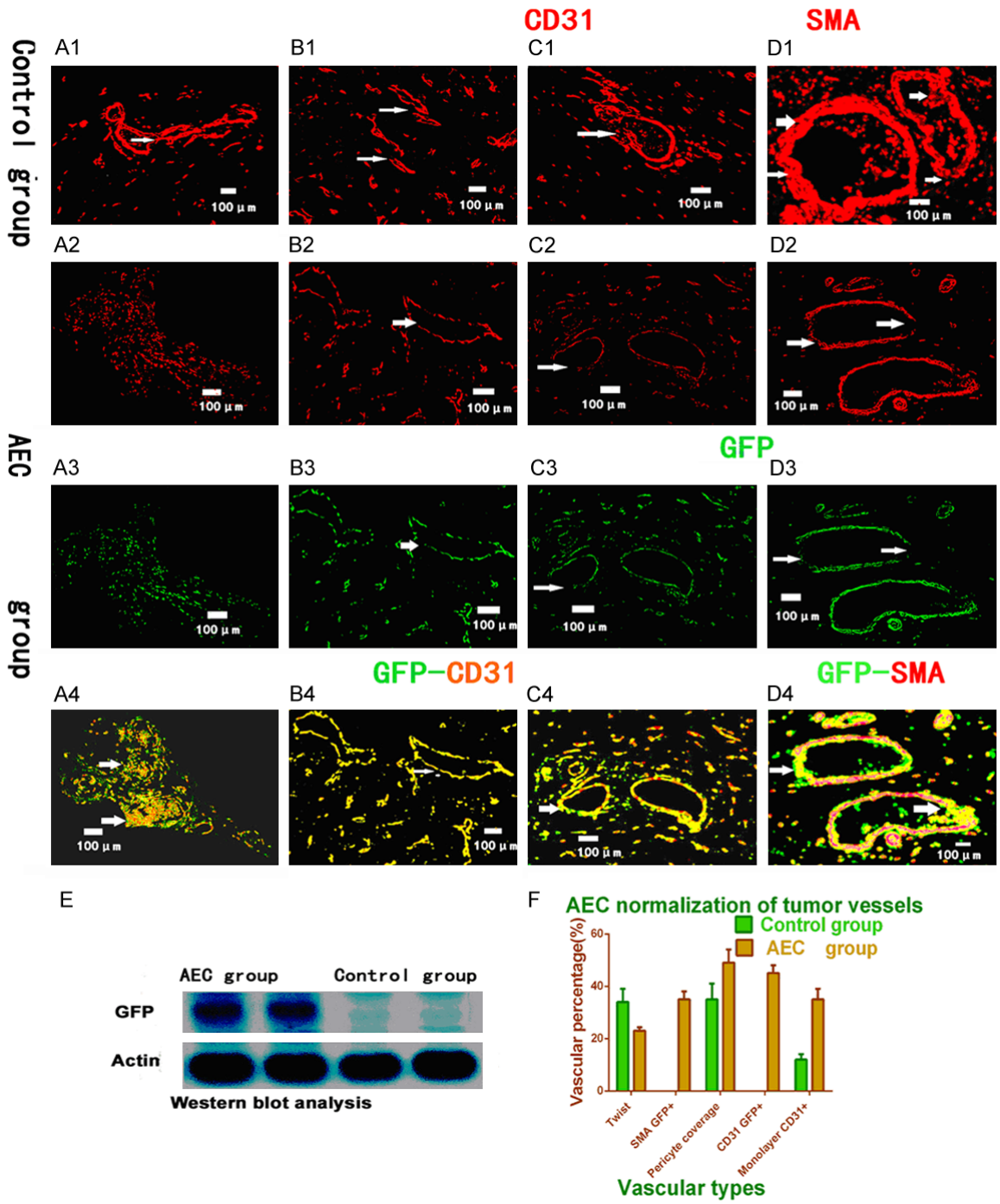

Figure 7. AECs restore uterine tumor vessels. (A1) The tumor vascular network was twisted, and the vascular structure was incomplete in the control group, with staining by CD31. (A2, A3) Tumor vessels in the AEC group, stained with CD31 and GFP. (A4) (A2) merged with (A3), CD31 and GFP(+) cells were colocalized in vascular networks with mural cells. AEC-GFP(+) cells were mixed with haemocytes within the microvascular cavity (arrow indicates). GFP(+) cells were integrated with endotheliocytes, and the microvascular wall and vascular structure integrity were enhanced. (B1) Tumor vessels sprouted to form new vessels with staining by CD31 in the control group, and the vascular structures were incomplete. (B2, B3) Tumor vascular staining by CD31 or GFP in the AEC group. (B4) (B2) merged with (B3), AEC-GFP(+) cells were integrated with tumors sprouting vessels (indicated by arrow). (C1) Monolayer endotheliocytes formed sites of vascularity with staining by CD31 in the control group. (C2, C3) Tumor vascular staining by CD31 or GFP in the AEC group. (C4) (C2) merged with (C3), monolayer endotheliocytes forming vascularity. GFP(+) coexisted with CD31(+) in the tumor matrix and at some sites of vascularity. GFP(+) cells were connected with endothelial cells labelled by CD31 within the tumor vascular network and lay on the same basement membrane. (D1)

Tumor vascular structures were incompletely labelled by SMA in the control group. (D2, D3) Tumor vascular staining by SMA or GFP in the AEC group. (D4) (D2) merged with (D3), SMA and GFP pericytes colocalized(+), and vascular structural integrity was enhanced (indicated by arrow). (E) GFP expression in uterine tumors was positive in the AEC group and negative in the control group by western blot. (F) The rate of tumor vascularity restoration by AECs.

In the AEC group, GFP(+) staining coexisted with CD31(+) staining in the tumor matrix and some tumor vessels. GFP(+) cells were closely connected with vascular endothelial cells labelled by CD31. GFP(+) AECs were appropriately integrated with the endothelial cells in a tumor vascular network and lay on the same basement membrane. Vascular structural integrity was clearly enhanced (see **Figure 7C2-C4**).

No GFP(+) cells were detected in the control group. The arrow indicates vascular structural defects in the control group by SMA staining (see **Figure 7D1**).

In the AEC group, SMA-GFP(+) cells were detected in pericytes around tumor vascularity, GFP(+) cells were colocalized with SMA(+) pericytes, and vascular structural integrity was increased significantly. Tumor vascularity GFP staining was positive, which confirmed that AECs participate in tumor revascularization. Sites of tumor vascularity became more mature than those in the control group (see **Figure 7D2-D4**). The proportion of pericyte-covered vessels was 35 ± 6% versus 49 ± 5% in the control group and AEC group, respectively. There was a significant difference between the two groups (two-way ANOVA, $F(1,56) = 6.426$, $P = 0.0141$, $n = 15$ for each group) (see **Figure 7F**).

GFP expression in uterine tumors was detected by western blot and was positive in the AEC group and negative in the control group. This finding confirmed that GFP-labelled AECs differentiated into tumor vascular components (endotheliocytes or pericytes) and stabilized the tumor vasculature (see **Figure 7E**).

In summary, GFP(+) cells were detected in tumor tissues after 5-30 days of AEC injection. Most CD31 or SMA GFP(+) vessels were detected in rat tumor uterine tissues. GFP(+) cells differentiated into tumor vascular endotheliocytes or pericytes and enhanced tumor vascular integrity. All of these results, including tumor tissue western blot of GFP and AEC luciferase IVIS imaging, proved that AECs homed to rat uterine tumor tissues after AEC injection. This finding confirmed that GFP(+) cells could migrate from the tail injection site and integrate into the tumor vascular wall to restore tumor vascular structures (see **Figure 7F**).

Discussion

Tumor vascular restoration and vascular tissue engineering

The process of vascular formation occurs during wound recovery, but vascular growth during wound recovery is closely monitored by vascular growth and inhibitory factors. Tumor vascular growth is out of control and forms blood vessels with leaky, twisted structures. Tumor cells can easily invade, escape from the tumor vasculature and resist antitumor treatment [8].

Tumor vascular endothelial cells are arranged in a disorder manner; few smooth muscle cells and pericytes encircle tumor vessels. Sites of tumor vascularity cannot respond to stimulation actively. Vascular perfusion dysfunction leads to tissue hypoxia. Thus, a tumor has been called a “wound that could not recover” [2, 9].

Many methods to inhibit tumor angiogenesis have been developed. The aim of current treatments has changed to repairing tumor vessels and enhancing vascular perfusion following chemotherapy or radiotherapy. Tumor vasculature restoration is regarded as another choice in tumor treatment. However, the prolonged vascular normalization time is a key issue.

The methods used to improve tumor vascular structure and function are called “vascular normalization”. These studies often block one signalling pathway that regulates tumor angiogenesis.

Pirfenidone enhances tumor vascular perfusion and reduces extracellular stroma elements by blocking the TGFβ signalling pathway [10].

Lenalidomide normalizes tumor vascularity by its immune-regulation and antiangiogenesis activity [11].

Chloroquine normalizes tumor vessels by blocking endothelial cell Notch 1 signalling [12].

Trastuzumab normalizes tumor vascularity by blocking VEGF-A expression [13].

Inositol trispyrophosphate normalizes tumor vascularity by the PTEN-PI3K-AKT signalling pathway [14].

These agents can only remodel tumor vascularity in a short period of time and cannot induce vascular homeostasis. Their effects are limited. Vascular tissue engineering may offer a new opportunity for tumor vascular restoration.

One approach to vascular tissue engineering is to use the release of angiogenic growth factors combined with extracellular matrix (ECM) and biochemical and mechanical signals to stimulate angiogenesis. The other approach is to use tissue-engineered vascular structures, which are made up of endothelial cells (ECs) alone or endothelial cells embedded in perivascular cells (PVCs) on ECM polymeric scaffolds. PVCs promote the stability of blood vessels by communicating with ECs, promoting the stability of blood vessels and binding them to the host circulation [15].

The task of vascular engineering is to look for different types of stem cells to form vascular structures to explore the mechanism of vascular growth. An important issue is how to provide a sufficient number of viable stem cells to repair abnormal tumor function and vasculature. The latter problem can be solved by adopting the methods of building vascular disease animal models and tracking stem cells and implanted vascular tissues by visualization and pathophysiologic techniques.

The strategy of angiogenesis and tissue regeneration is still in its infancy. To generate blood vessels with proper mechanical strength and function, the source of vascular cells, as the key to engineering blood vessels, still faces many challenges and obstacles.

Stem cell choice and advantages of AECs

The determinants of efficient stem cell selection are an abundant source, easy separation and a high proliferation rate.

Autologous mature vascular cells are the basis of vascular tissue engineering, but they are limited by cell quantity and quality.

Adult stem cells are a promising source of cells in vascular tissue engineering. Their advantage is that they can be easily obtained from various tissues, and their in vitro cell culture time is short, with differentiation into smooth muscle cells or ECs without the risk of tumorigenesis. The largest obstacle to their application is that cell senescence and differentiation ability decrease as the donor age increases.

It was reported [16] that vascular remodelling is triggered by tumor growth, inflammation, and hypoxia surrounding blood vessels. Nestin(+) multipotential stem cells that originate from the vascular adventitia can move towards the tumor tissues, differentiate into smooth muscle cells, rebuild the tumor vasculature and stabilize the tumor vasculature.

Mesenchymal stem cells (MSCs) are derived from the mesoderm. MSCs possess the ability to self-renew and undergo multidirectional differentiation, so MSCs can be used in tissue regeneration and repair. It was found that MSCs have the characteristics of targeted migration to tumor sites, homing to tumor tissue and differentiating into interstitial tissue, changing the tumor microenvironment and affecting tumor growth and metastasis. MSCs not only have good targeting ability to tumor cells but also promote tumor interstitial remodelling and tumor angiogenesis. Kéramidas et al. reported [17] that MSCs separated from human bone marrow could inhibit mouse adenocarcinoma growth, modify the tumor vasculature, and decrease the number of blood vessels while enhancing vascular length.

Bone marrow stem cells are rare and obtained by invasive methods. Other readily available tissues include adipose tissue and placental tissue, including the umbilical cord, amniotic membrane, and amniotic fluid.

At present, *embryonic stem cells* (ESCs) are still the gold standard for pluripotent stem cells. Other stem cells need to be compared with ESCs in terms of their functional properties. However, the application of ESCs is subject to ethical limitations, and immune rejection may occur because of separation from embryos. Endothelial progenitor cells that originated from ESCs could repair tumor vessels and correct tumor hypoxia [17].

Collet et al. [18] isolated and obtained endothelial progenitor cells from mouse embryos. This cell line could bind to mature ECs to form tube-like structures and invade tumor spheroids to form vascular structures. Endothelial progenitor cells were transfected and expressed the VEGFR2 gene. Intravenous injection of this cell line could correct hypoxia in mouse tumor tissue.

Yamanaka et al. transformed the transcription factors Oct4, Sox2, Klf4 and c-Myc into somatic cells by viral vectors and induced somatic fibroblasts into pluripotent stem cells. ESCs are like pluripotent cells obtained by reprogramming. By introducing exogenous genes, somatic cells could be differentiated into pluripotent stem cells, so the cells were called *induced pluripotent stem cells* (IPSCs). This technology reversed the differentiation of somatic cells to generate stem cells, which changed people's understanding of stem cells and provided a new way to obtain stem cells [19].

There are no ethical problems related to the use of IPSCs. IPSCs can be reprogrammed from the patient's somatic cells and possess ESC angiogenesis ability.

The problems associated with IPSC application are outlined below [20, 21].

Risk of tumorigenesis and mutation

Since the c-myc gene was introduced into IPSCs, IPSC have a risk of tumorigenesis, with the formation of teratomas or other tumors at the IPSC graft site or away from the graft site because the viral vectors used can be permanently integrated into random sites in the genome. As the virus vectors used can be randomly and permanently integrated into the genome, gene mutation may be caused by reprogramming with virus, genomic integration, and accumulation of chromosomal abnormalities, which holds risks for the application of IPSCs in clinical treatment.

Non-traditional reprogramming methods with non-traditional plasmids, mRNA, proteins or small molecules have been used to promote the production of IPSCs and reduce gene toxicity. However, IPSCs induced without viral integration methods remain in non-methylated conditions; this condition is prone to tumorigenesis.

Low differentiation efficiency

Since the mechanism of IPSC transformation is not completely understood, the differentiation efficiency of IPSCs is very low. IPSCs are very inefficient and require enough cells to be transplanted. Therefore, more efficient methods should be explored.

Immunological rejection

Although IPSCs can be transformed from patient somatic cells, it is not clear whether their immunogenicity changes during cell reprogramming.

Differences in cell sources

What factors determine the subsequent differentiation potential of IPSCs? Cell source, the efficiency of reprogramming protocols, or both? With increasing donor age, cell senescence and differentiation ability decrease. IPSC-differentiated cells may mutate. Are IPSC characteristics the same in different tissues? Answers remain unclear.

Thus far, the protocols for establishing IPSCs in various laboratories are different. A consensus on how to quickly obtain mature and stable IPSCs needs to be reached.

The above difficulties impede the clinical application of IPSCs.

Advantages of AECs as pluripotent stem cells [22, 23]

AECs originate from discarded placental tissues and are easy to obtain. There are no ethical controversies. No implantation rejection reaction occurs. Due to a lack of telomeres, no teratomas form within the host. AECs possess the ability to differentiate into embryonic endoderm, mesoderm and ectoderm layers.

AECs come from placental epithelial tissue and maintain pluripotent stem cell characteristics. The characteristics of AECs lie between those of embryonic and mature stem cells. AECs are the most promising seed cell resource in the field of regenerative medicine. AECs were selected as a candidate new stem cell source and

as one of the top ten medical breakthroughs of 2007 in the American Time Magazine [23].

AECs are a good choice for tissue engineering, and no implant rejection occurred in the above experimental endometrial cancer model.

It was reported [5] that human amniotic fluid stem cells always combined with nude mouse respiratory tract cells and changed into alveolar and bronchiolar epithelial cells in mouse lungs subjected to different types of lung damage.

Wang reported [6, 24] that intravenously injected AECs migrated to mouse ovaries and differentiated into granulocytes. Ovarian tissues were stained by an immunofluorescent antibody specific for human antigen and by GFP, which colocalized in ovarian tissues. The amount of Müllerian hormone increased, and ovarian follicular function was restored.

AECs restore vascular homeostasis in endometrial tumors

AECs are used in tissue engineering to increase blood perfusion and promote wound healing. There are no reports on the use of AECs in treatment for "tumor vascular restoration".

One aim of this study was to evaluate the pluripotent stem cell features of AECs, and another aim was to determine whether AECs can enhance tumor vascular integrity and restore vascular homeostasis.

In this study, the expression of the pluripotent stem cell markers Nanog, Oct-4, CD117, Rex-1 and SSEA4 in AECs was detected by immunofluorescence, RT-PCR and western blot. AECs were induced to differentiate into adipose, osteogenic, and chondrogenic cells.

To explore the vasculogenic abilities of AECs, AEC vascular formation features were tracked in vitro and in vivo. AECs were transfected with lentiviral-GFP-luciferase (Luc). GFP-labelled AECs formed vascular tube-like structures and invaded tumor tissue to form vascular structures in vitro. A nude rat in situ endometrial cancer model was built, and luciferase kinetic imaging confirmed that AECs homed to rat uterine tumor tissues after injection by the rat tail vein.

In this study, GFP-Luc-labelled AECs were injected, and the ability of AECs to restore the rat vascular structure and perfusion function in endometrial cancer were evaluated.

AECs restored the tumor vascular structure. The ratio of α-SMA/CD31 (VMI) increased. The content of cadherin in tumor tissues increased. AECs regulated the unusual thickening of the basement membrane and enhanced vascular basement membrane integrity. The decrease in VEGF-A expression in the AEC group demonstrated that AECs inhibited abnormal tumor vascular hyperplasia.

AECs increased the blood perfusion fraction, corrected tumor tissue anoxia and decreased blood vessel leakage. Detected by Hoechst 33342 vascular perfusion and ultrasonic CDFI, the tumor perfusion fraction of the tumor was enhanced after AEC injection. Detected by pimonidazole, tumor tissue hypoxia declined after AEC injection.

In this study, the tumor proliferative ratio and tumor volume further decreased in the AEC + DDP group. Tumor apoptosis and the rat survival rate in the AEC + DDP group were further enhanced. This finding proved that AECs enhanced the cytotoxic effect of DDP in endometrial cancer cells. This effect corresponds to the tumor vascular morphology and perfusion normalizing changes induced by AECs. AECs improved vascular formation in tumors.

Why did the tumor volume in the AEC group not surpass that of the control group? As previously reported [17], bone marrow stem cells can inhibit mouse adenocarcinoma growth and modify the tumor vasculature. We speculate that AECs may have a slight inhibitory effect on tumor growth, but this possibility requires further exploration.

In this study, we performed kinetic luciferase IVIS imaging, tumor western blot analysis of GFP and tumor GFP + CD31 (or SMA) immunofluorescence double staining. AECs circulated into the rat tumor tissues and integrated with the tumor vascular structure to form efficient tumor vascular networks after 30 days. AECs combined with host tumor vascular ECs or integrated with smooth muscle cells. AECs combined with tumor vascular lumen cells of different tube diameters and enhanced vascular integrity, confirming that AECs could home to sites of tumor vasculogenesis and become a

constituent of the vasculature. Therefore, AECs increased tumor blood perfusion, reduced hypoxia and enhanced the cytotoxic effect of DDP. We speculate that AECs may be attracted by some chemicals from endometrial cancer and migrate into tumor tissues, but this possibility requires further exploration.

Conclusions

This study confirmed that AECs have vascular formation ability and stem cell features. AECs could form vascular-like structures in vitro, home to endometrial cancer tissues, integrate into the tumor vascular lumen, differentiate into ECs or smooth muscle cells, restore tumor vascular homeostasis, and enhance vascular perfusion and the cytotoxic effects of DDP. Therefore, AECs may offer a new approach for rebuilding tumor vascularity. However, the detailed mechanism by which AECs home to the tumor tissue and differentiate into vascular components still needs further exploration.

Acknowledgements

This study was approved by the ethics committee of Zhabei Central Hospital (No. 2017-98). All donors of placentas provided written informed consent to participate in the study. There were no conflicts of interest. The authors thank medical staff from Zhabei Central Hospital for their advice and cooperation. The authors thank Professor Yi Tan and his postgraduate Genling Yang from Chongqing Medical University in China for their help with the nude rat experimental technology. The authors thank Cruilife Stem Cell Group Limited in China for their help with stem cell culture technology. The authors thank Professor Yuezhi Zhang and Professor Xiaohan Wang from Chifeng Second Hospital for their help with pathology experiment technology.

Disclosure of conflict of interest

None.

Abbreviations

AEC, Amniotic epithelial cells; ANOVA, Analysis of variance; CDFI, Color doppler flow imaging; CK19, Cytokeratin 19; DAPI, 4,6-Diamino-2-phenyl indole; DDP, cis-Dichlorodiammine platinum; ECM, Extracellular matrix; ECs, Endothelial cells; ELISA, Enzyme-linked immunosorbent assay; ESC, Embryonic stem cell; GFP, Green fluorescent protein; H&E, Hematoxylineosin; IPSC, Induced pluripotent stem cells; IVIS, In vivo images system; Luc, Luciferase; MVD, Microvessel density; MSC, Mesenchymal stem cells; PVCs, Perivascular cells; PBS, Phosphate buffered saline; RNA, Ribose nucleic acid; RT-PCR, Reverse transcription-polymerase chain reaction; TGF, Transforming growth factor; TUNEL, Transferase-mediated deoxyuridine triphosphate-biotin nick end labeling; VEGF, Vascular endothelial growth factor; VMI, Vascular maturation index.

Address correspondence to: Liming Guan, Department of Obstetrics and Gynaecology, Zhabei Central Hospital, No. 619, Zhonghuaxin Road, Jing'an District, Shanghai 200000, China. E-mail: guanliming1@126.com

References

[1] Wang ZW. Broad targeting of angiogenesis for cancer prevention and therapy. Semin Cancer Biol 2015; 35: S224-S243.

[2] Goel S, Duda DG, Xu L, Munn LL, Boucher Y, Fukumura D, Jain RK. Normalization of the vasculature for treatment of cancer and other diseases. Physiol Rev 2011; 91: 1071-1121.

[3] Guan L. Angiogenesis dependent characteristics of tumor observed on rabbit VX2 hepatic carcinoma. Int J Clin Exp Pathol 2015; 8: 12014-12027.

[4] Guan L, Xu G. Damage effect of high-intensity focused ultrasound on breast cancer tissues and their vascularities. World J Surg Oncol 2016; 14: 153.

[5] Carraro G, Perin L, Sedrakyan S, Giuliani S, Tiozzo C, Lee J, Turcatel G, De Langhe SP, Driscoll B, Bellusci S, Minoo P, Atala A, De Filippo RE, Warburton D. Human amniotic fluid stem cells can integrate and differentiate into epithelial lung lineages. Stem Cells 2008; 26: 2902-2911.

[6] Wang F, Wang L, Yao X, Lai D, Guo L. Human amniotic epithelial cells can differentiate into granulosa cells and restore folliculogenesis in a mouse model of chemotherapy-induced premature ovarian failure. Stem Cell Res Ther 2013; 4: 124.

[7] Guan L, Xu G. Destructive effect of HIFU on rabbit embedded endometrial carcinoma tissues and their vascularities. Oncotarget 2017; 8: 19577-19591.

[8] Finocchario-Kessler S, Wexler C, Maloba M, Mabachi N, Ndikum-Moffor F, Bukusi E. Cervical cancer prevention and treatment research in Africa: a systematic review from a public health perspective. BMC Womens Health 2016; 16: 29.

[9] Westin SN, Broaddus RR. Personalized therapy in endometrial cancer: challenges and opportunities. Cancer Biol Ther 2012; 13: 1-13.
[10] Polydorou C, Mpekris F, Papageorgis P, Voutouri C, Stylianopoulos T. Pirfenidone normalizes the tumor microenvironment to improve chemotherapy. Oncotarget 2017; 8: 24506-24517.
[11] Leuci V, Maione F, Rotolo R, Giraudo E, Sassi F, Migliardi G, Todorovic M, Gammaitoni L, Mesiano G, Giraudo L, Luraghi P, Leone F, Bussolino F, Grignani G, Aglietta M, Trusolino L, Bertotti A, Sangiolo D. Lenalidomide normalizes tumor vessels in colorectal cancer improving chemotherapy activity. J Transl Med 2016; 14: 119.
[12] Maes H, Kuchnio A, Peric A, Moens S, Nys K, De Bock K, Quaegebeur A, Schoors S, Georgiadou M, Wouters J, Vinckier S, Vankelecom H, Garmyn M, Vion AC, Radtke F, Boulanger C, Gerhardt H, Dejana E, Dewerchin M, Ghesquière B, Annaert W, Agostinis P, Carmeliet P. Tumor vessel normalization by chloroquine independent of autophagy. Cancer Cell 2014; 26: 190-206.
[13] Sorace AG, Quarles CC, Whisenant JG, Hanker AB, McIntyre JO, Sanchez VM, Yankeelov TE. Trastuzumab improves tumor perfusion and vascular delivery of cytotoxic therapy in a murine model of HER2+ breast cancer: preliminary results. Breast Cancer Res Treat 2016; 155: 273-284.
[14] Kieda C, El Hafny-Rahbi B, Collet G, Lamerant-Fayel N, Grillon C, Guichard A, Dulak J, Jozkowicz A, Kotlinowski J, Fylaktakidou KC, Vidal A, Auzeloux P, Miot-Noirault E, Beloeil JC, Lehn JM, Nicolau C. Stable tumor vessel normalization with pO2 increase and endothelial PTEN activation by inositol trispyrophosphate brings novel tumor treatment. J Mol Med (Berl) 2013; 91: 883-99.
[15] de Girolamo L, Lucarelli E, Alessandri G, Avanzini MA, Bernardo ME, Biagi E, Brini AT, D'Amico G, Fagioli F, Ferrero I, Locatelli F, Maccario R, Marazzi M, Parolini O, Pessina A, Torre ML; Italian Mesenchymal Stem Cell Group. Embryonic stem cell: a new "cells as drugs" paradigm. Efficacy and critical aspects in cell therapy. Curr Pharm Des 2013; 19: 2459-2473.
[16] Klein D, Meissner N, Kleff V, Jastrow H, Yamaguchi M, Ergün S, Jendrossek V. Nestin(+) tissue-resident multipotent stem cells contribute to tumor progression by differentiating into pericytes and smooth muscle cells resulting in blood vessel remodeling. Front Oncol 2014; 4: 169.
[17] Kéramidas M, de Fraipont F, Karageorgis A, Moisan A, Persoons V, Richard MJ, Coll JL, Rome C. The dual effect of mesenchymal stem cells on tumor growth and tumor angiogenesis. Stem Cell Res Ther 2013; 4: 41.
[18] Collet G, Szade K, Nowak W, Klimkiewicz K, El Hafny-Rahbi B, Szczepanek K, Sugiyama D, Weglarczyk K, Foucault-Collet A, Guichard A, Mazan A, Nadim M, Fasani F, Lamerant-Fayel N, Grillon C, Petoud S, Beloeil JC, Jozkowicz A, Dulak J, Kieda C. Endothelial precursor cell-based therapy to target the pathologic angiogenesis and compensate tumor hypoxia. Cancer Lett 2016; 370: 345-57.
[19] Klein D. iPSCs-based generation of vascular cells: reprogramming approaches and applications. Cell Mol Life Sci 2018; 75: 1411-1433.
[20] Rufaihah AJ, Huang NF, Kim J, Herold J, Volz KS, Park TS, Lee JC, Zambidis ET, Reijo-Pera R, Cooke JP. Human induced pluripotent stem cell-derived endothelial cells exhibit functional heterogeneity. Am J Transl Res 2013; 5: 21-35.
[21] Yang L, Geng Z, Nickel T, Johnson C, Gao L, Dutton J, Hou C, Zhang J. Differentiation of human induced-pluripotent stem cells into smooth-muscle cells: two novel protocols. PLoS One 2016; 11: e0147155.
[22] Benavides OM, Brooks AR, Cho SK, Petsche Connell J, Ruano R, Jacot JG. In situ vascularization of injectable fibrin/poly (ethylene glycol) hydrogels by human amniotic fluid-derived stem cells. J Biomed Mater Res A 2015; 103: 2645-2653.
[23] Mirabella T, Hartinger J, Lorandi C, Gentili C, van Griensven M, Cancedda R. Proangiogenic soluble factors from amniotic fluid stem cells mediate the recruitment of endothelial progenitors in a model of ischemic fasciocutaneous flap. Stem Cells Dev 2012; 21: 2179-88.
[24] Zhang Q, Xu M, Yao X, Li T, Wang Q, Lai D. Human amniotic epithelial cells inhibit granulosa cell apoptosis induced by chemotherapy and restore the fertility. Stem Cell Res Ther 2015; 6: 152.